

# TQSim: A Case for Reuse-Focused Tree-Based Quantum Circuit Simulation

Meng Wang  
mengwang@ece.ubc.ca  
Univ. of British Columbia  
Vancouver, Canada

Rui Huang  
huangrui@cs.wisc.edu  
University of Wisconsin  
Madison, USA

Swamit Tannu  
swamit@cs.wisc.edu  
University of Wisconsin  
Madison, USA

Prashant Nair  
prashantnair@ece.ubc.ca  
Univ. of British Columbia  
Vancouver, Canada

**Abstract**—Quantum computers can speed up computationally hard problems. However, to realize their full potential, we must mitigate qubit errors (from noise) by developing noise-aware algorithms, compilers, and architectures. Thus, simulating quantum programs on classical computers with different noise models is a de-facto tool that is used by researchers and practitioners. Unfortunately, noisy quantum simulators iteratively execute the same circuit across multiple trials (shots) – thereby incurring high-performance overheads.

To address this, we propose a noisy simulation technique called Tree-Based Quantum Circuit Simulation (TQSim). TQSim exploits the reusability of the intermediate results during the noisy simulation and reduces computation. TQSim dynamically partitions a circuit into several subcircuits. It then reuses the intermediate results from these subcircuits during computation. As compared to a noisy Qulacs-based baseline simulator, TQSim achieves an average speedup of  $2.51\times$  across 48 different benchmark circuits. Additionally, across benchmarks, TQSim produces results with a normalized fidelity that is within 0.016 range of the baseline normalized fidelity.

## I. INTRODUCTION

Lately, quantum computing (QC) hardware has achieved impressive results [2], [47], [50]. Several works have demonstrated the value of QC in cryptography [38], unstructured database search [18], and quantum system simulation [29]. However, access to real quantum computers continues to be limited, with industry players having around just over 20 quantum systems [23]. Quantum circuit simulation is seen as a mechanism that helps developers accelerate and validate QC-related research and overcome these constraints [19]. However, simulating gate-based quantum circuits is challenging. This is because, as the number of qubits in a quantum circuit grows, its computational state space also grows exponentially. What makes quantum circuit simulation even more challenging is the necessity to incorporate the effect of noise, i.e. the noisy simulation.

Quantum algorithms designed for near-term Noisy Intermediate-Scale Quantum (NISQ) computers rely on simulations that try to mimic the effect of noise in physical quantum computers. Quantum simulators, while employing multiple shots, could take up to  $100\times$  higher execution time to simulate noisy quantum circuits. Previous optimization techniques for quantum circuit simulation [16], [42], [44], [48] and parallelization methods, i.e. multiprocessing and GPU simulation, focus on improving the performance of

the single-shot simulation process. We observe that there exists significant room for improving the performance of the multi-shot simulation process. The goal of this paper is to design a performance-efficient simulator for NISQ-era quantum algorithms and quantum computers.

Figure 1 shows the simulation time of the 15-qubit Quantum Fourier Transform (QFT) circuit for ideal and noisy simulation while executing on two 16-core Intel® Xeon® 6130 processors. The simulation time for the noisy circuits is  $170\times$  to  $335\times$  higher than that for the ideal circuits.

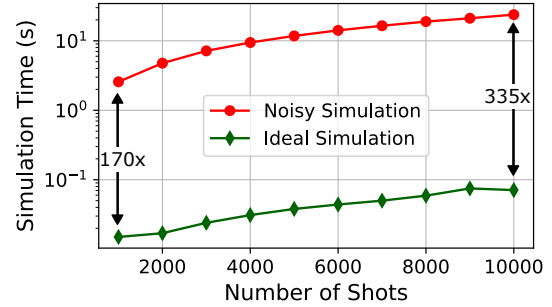


Fig. 1: Simulation time (in seconds) of ideal and noisy simulation for a 15-qubit Quantum Fourier Transform (QFT) circuit while executing on two 16-core Intel® Xeon® 6130 processors. The simulation time of the noisy circuits is  $170\times$  to  $335\times$  higher than that for the ideal circuits.

This is because noisy simulations perform multiple trials (shots) as the final outcome distribution of a NISQ machine tends to vary due to noisy qubits. Therefore, the final outcome is sampled from a noisy-version of the ideal distribution. Thus, to improve fidelity, we need a sufficient number of outcomes in order to recover the original distribution. In practice, depending on the quantum circuit, up to 10,000+ simulation shots would have to be evaluated.

Figure 2a shows the noise-free circuit and the possible noise operators used in the noisy simulation. Figure 2b shows the noisy circuits generated for a 4-shot noisy simulation task. These circuits are generated by inserting noise operators into the original circuit. This paper observes that there is *computation reuse* across multiple shots in such circuits. For example, parts of the four noisy circuits, labelled by the dash

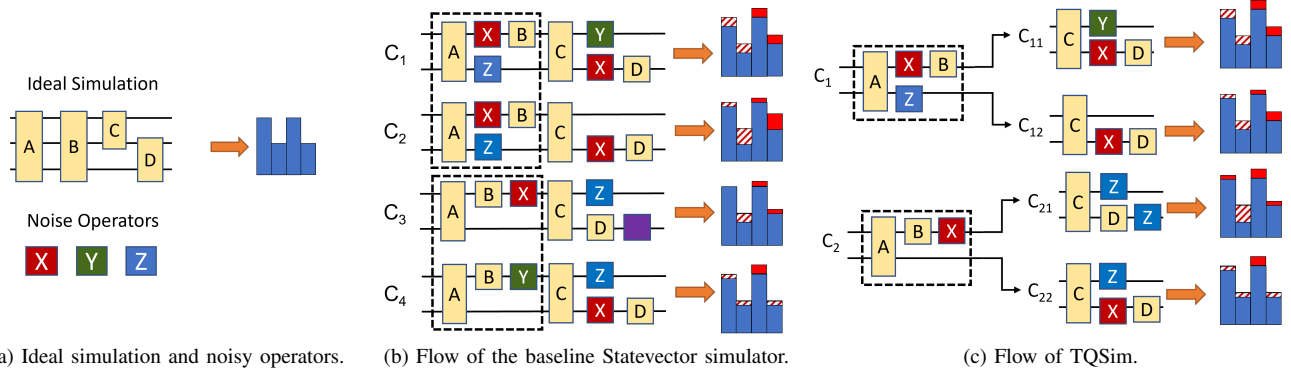


Fig. 2: Noisy circuits and potential reuse of the intermediate states<sup>1</sup>. (a) Ideal simulation and possible noise operators. (b) Four noisy circuits are generated from the original circuit and their noisy-version resulting distributions. (c) Reuse the intermediate state after Gate B and the new noisy-version resulting distributions.

lines in Figure 2b, have similar noisy operators. For those parts, modern NISQ simulators tend to repeat similar computations across multiple shots. Fortunately, one can reduce the computation by reusing these intermediate states. Figure 2c shows the noisy circuits when we reuse the intermediate states after gate B. This could reduce the total computation by 25%. Based on this insight, this paper presents a tree-based quantum circuit simulator called TQSim. TQSim is a Statevector-based simulator that reuses intermediate states to speed up noisy quantum simulation on a classical computer.

TQSim partitions the quantum circuit into subcircuits and executes them separately. The resulting subcircuit states, except for the one from the last subcircuit, are called intermediate states. TQSim reuses the intermediate states across multiple simulation shots. For instance, the circuit in Figure 2 has two subcircuits - the first one contains gates A, B and the second one contains gates C, D. The resulting state from the first subcircuit is thus reused twice.

TQSim faces two key challenges. First, decide how to efficiently partition the quantum circuit. Second, determine the number of reuses for each intermediate state. We observe that if we generate a large number of subcircuits, we can achieve an increasingly high speedup. However, it also requires a large memory capacity, as several more intermediate states would now need to be stored. Furthermore, if we can increase the *reuse* for these intermediate states, we can achieve significant performance gains. However, naively increasing the number of reuses can reduce the accuracy of the final result. Therefore, we need to maintain a balance between the obtainable speedups and desired final accuracy of the noisy quantum circuit simulator.

To address these challenges, TQSim proposes a dynamic circuit partition (DCP) technique that dynamically determines the circuit partitions and shot distributions according to the error rates and gate count of the circuit. This enables DCP to obtain a high speedup while producing results that are close

to ones obtained from a precise noisy simulator.

We evaluate TQSim using 48 quantum circuits from 8 different circuit classes. We show that TQSim can have up to  $3.89\times$  speedup over baseline implementation for noisy simulation. On average, TQSim provides an average speedup of  $2.51\times$ . Furthermore, TQSim produces a result with a normalized fidelity that is within 0.016 range of the normalized fidelity of baseline result. On average, the difference between TQSim normalized fidelity and baseline normalized fidelity is 0.006.

## II. BACKGROUND AND MOTIVATION

### A. Quantum Computing: Bits and Gates

A quantum bit or qubit is the basic unit in quantum computing (QC). Its state,  $|\psi\rangle$ , can be expressed as:

$$|\psi\rangle = \alpha|0\rangle + \beta|1\rangle$$

Here  $|0\rangle$  and  $|1\rangle$  are two basis states that are orthogonal to each other and the  $\alpha$  and  $\beta$  are their corresponding probability amplitudes. For an  $n$ -qubit quantum system, there are  $2^n$  basis states, therefore, the number of amplitudes for the  $n$ -qubit system is  $2^n$ . The state of a given qubit system is generally expressed as a Statevector, of all the amplitudes.

### B. Quantum Computing: Circuits

Quantum algorithms are expressed as circuits. A circuit is a list of quantum gates that need to be applied, in order, to modify the initial quantum state. Similarly, a quantum subcircuit is a consecutive sub-list of the original list of gate operations in the circuit. The five commonly used gates are,  $X$ ,  $Y$ ,  $Z$ , *Hadamard* ( $H$ ), and *CNOT*.

### C. Ideal Quantum Circuit Simulation

An ideal quantum circuit simulator multiplies the matrix representations of the quantum gates in the given circuit to the initial Statevector. The resulting Statevector is deemed as

<sup>1</sup>The listed noise operators are for depolarizing error channels. We evaluate TQSim with several other error channels listed in Section IV and the results are shown in Section V.

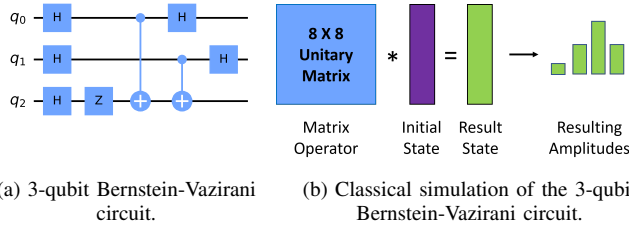


Fig. 3: Quantum circuit for the Bernstein-Vazirani algorithm and equivalent computation for its classical simulation.

the final state of the simulator from which the final outcome is sampled. We use the Bernstein–Vazirani (BV) algorithm [5], shown in Figure 3a, to describe the computation in a quantum circuit simulation. As shown in Figure 3b, the unitary matrix represents the gates and their interactions. This matrix is multiplied with a Statevector that describes the initial state. The outcome is sampled from the resulting Statevector.

#### D. Noisy Quantum Circuit Simulators: Taxonomy

Broadly, there are two practical methods for performing noisy quantum circuit simulation.

1) *Density Matrix Simulator*: A Density Matrix can be used to represent mixed states. It can be obtained by Equation 1 as shown below:

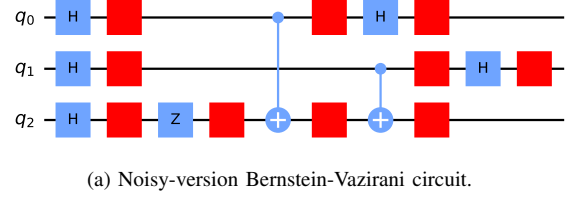
$$\rho = \sum_i p_i |\psi_i\rangle \langle \psi_i| \quad (1)$$

where the  $p_i$  is the probability of  $|\psi_i\rangle$ . The size of the Density Matrix is  $2^n \times 2^n$  (where ‘n’ is the number of qubits). Thus its memory usage increases double exponentially with the number of qubits. As Density Matrix can represent mixed states, for noisy simulation, it only requires one full simulation and all the required outcomes can be sampled from the same resulting Density Matrix. However, the memory usage of the Density Matrix simulator limits its usability.

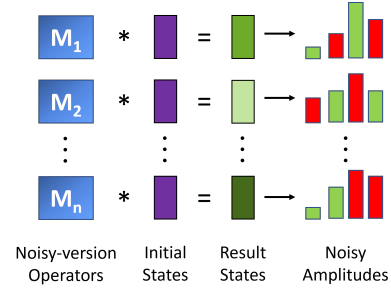
2) *Statevector Simulator*: Statevector simulation helps overcome the memory capacity overheads of the Density Matrix simulation technique. In the Statevector method, the Statevector that represents the initial state is multiplied by the matrix operator (described in Section II-C). The size of the Statevector is  $2^n$ , which has  $2^n \times$  lower memory usage as compared to the Density Matrix simulator. As the Statevector can only represent pure quantum states, for noisy simulation, a Statevector simulator repeats the whole simulation process across several thousands of shots.

#### E. Noisy Simulation Using Statevector Simulator

The noisy-version of the quantum circuit is generated by inserting noise operators into the original quantum circuit [4]. Figure 4a shows the potential locations in the original circuit for these noise operators. Figure 4b shows the computations performed for the noisy simulation. This linear increase in computations with respect to the number of shots intuitively explains the performance overheads.



(a) Noisy-version Bernstein-Vazirani circuit.



(b) Computations for the noisy simulation.

Fig. 4: Noisy circuits and computations for the noisy simulation of the Bernstein-Vazirani circuit. (a) The noisy-version Bernstein-Vazirani circuit with possible noise operators is highlighted in red. (b) The noisy operators vary the unitary matrices ( $M_1, M_2, \dots, M_n$ ) and produce several different resulting states across several shots.

#### F. Quantifying the Overheads in Noisy Circuit Simulators

The main limitation of the Density Matrix simulator is its memory usage which is  $\mathcal{O}(2^{2n})$ . As shown in Figure 5, the memory usage of Density Matrix is exponentially greater than the Statevector method (which is  $\mathcal{O}(2^n)$ ). For instance, for a quantum state with 16 qubits, the Statevector simulator requires only 1MB memory capacity while the Density Matrix simulator requires ~64GB of memory capacity.

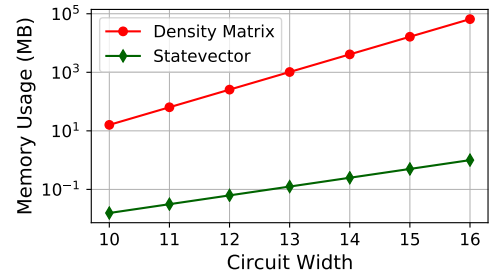


Fig. 5: The memory usage for the Density Matrix simulator and Statevector simulator with varying circuit widths. The Density Matrix simulator requires  $2^n \times$  higher memory capacity as compared to the Statevector simulator.

Figure 6 shows the single-shot execution time for the Density Matrix and the Statevector simulators. The execution time of the Density Matrix simulator is several times greater than the Statevector simulator. For instance, for a circuit width of 16, the Statevector and the Density Matrix simulators require 9ms and 1788 seconds respectively executing on two 16-core Intel® Xeon® 6130 processors. Thus, for enabling a scalable simulation tool, we select the Statevector simulator to implement our proposal.

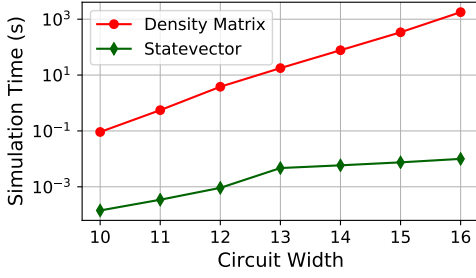


Fig. 6: The simulation time for the Density Matrix simulator and Statevector simulator with varying circuit widths running on two 16-core Intel® Xeon® 6130 processors. The Density Matrix simulator can incur up to  $10^4 \times$  higher simulation time as compared to the Statevector simulator.

### III. DESIGN: TREE-BASED QUANTUM SIMULATOR

This section presents the design of the Tree-Based Quantum Circuit Simulator (TQSim). TQSim uses a *circuit partitioner* to divide the given quantum circuit into subcircuits and determines the number of shots for each subcircuit.

Figure 7a shows the three-subcircuit representation of the 3-qubit BV circuit. For this representation, Figure 7b shows the simulation tree when using the baseline simulator. The simulation tree has the following characteristics. First, the root node is the initial state,  $|\psi_i\rangle$ . Second, the internal nodes with depth of  $i+1$  represent the  $i_{th}$  subcircuit. Third, the arity of a given node indicates the number of reuses of the resulting state from that subcircuit. For example, in the baseline simulation, we have no reuses, therefore, the arity of all the nodes in Figure 7b is 1 except for the root node.

#### A. TQSim: Organization

TQSim creates a simulation tree with nodes on the same layer all having the same arity. We use the following notation for the tree structure (assuming  $k$  subcircuits):

$$(A_0, A_1, \dots, A_{k-1})$$

The  $A_i$  is the arity of the nodes with a depth of  $i$ . For example, as the baseline simulation shown in Figure 7b incurs 64 shots, its simulation tree can be represented as (64,1,1). In this representation, we can calculate the number of instances of  $i_{th}$  subcircuit using the following equation:

$$i_{th} \text{ Subcircuit Instances} = \prod_{j=0}^{i-1} A_j \quad (2)$$

The total number of outcomes of a TQSim simulation tree, therefore, is  $\prod_{j=0}^{k-1} A_j$ .

#### B. Dynamic Circuit Partition (DCP)

1) *Motivation*: A straightforward and naive technique would be to equally partition the quantum circuit into  $k$  subcircuits and uniformly distribute the shots. However, in this method, the total number of nodes increases exponentially as the depth of the tree increases. For example, if we have 3 subcircuits with 1000 total shots, we end up with an TQSim tree structure of (10,10,10). This results in the first subcircuit

being simulated 10 times, the second subcircuit 100 times, and the third subcircuit 1000 times. We can see there is a large gap between the number of instances for each subcircuit with the front subcircuits having very few instances and potentially reducing the accuracy. To address this, we propose a Dynamic Circuit Partition (DCP) method that actively determines the number of shots for the first subcircuit based on the given error rates and tries to provide speedup while maintaining accuracy.

2) *The First Subcircuit*: In the TQSim design, the first subcircuit is the portion of the original circuit that gets simulated the least number of times. Therefore, it is vital to determine how many shots we need to allocate for the first subcircuit. To ensure both near-optimal speedups and accuracy, we generate the first subcircuit with the minimum number of gates - determined based on the state copy overhead and will discuss more in detail in Section III-C. We then calculate its overall error rate using Equation 3.

$$\text{First Subcircuit Error Rate} = 1 - \prod_i (1 - e_i) \quad (3)$$

Where  $e_i$  are the probabilities of inserting a noise operator after each of the gates in the first subcircuit. We use this error rate to calculate the number of shots for the first subcircuit such that we achieve very high accuracy and speedup. To this end, we reuse the concept of statistical sampling on the total number of shots [35].

For our analysis, we can consider that a part of the whole population involved in sample size calculation is of a special type. Specifically, the whole population is the total number of shots and the special type of population are the noisy circuits. The proportion of the noisy circuits is equal to the error rate of the first subcircuit. We calculate the number of shots for the first subcircuit with a confidence level of 95% and 5% margin of error using Equation 4 given below:

$$A_0 \geq \frac{z^2 * \hat{p}(1 - \hat{p})}{\varepsilon^2} * \frac{1}{1 + \frac{z^2 * \hat{p}(1 - \hat{p})}{\varepsilon^2 N}} \quad (4)$$

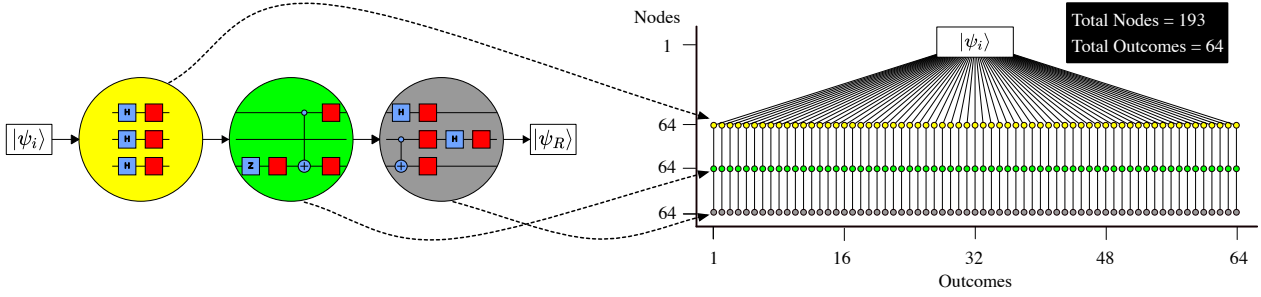
Where ‘ $z$ ’ is the z-score of the given confidence level,  $\varepsilon$  is the margin of error, ‘ $N$ ’ is the total number of shots, and  $\hat{p}$  is the overall error rate of the first subcircuit.

3) *Remaining Subcircuits*: Since the shot calculation for the first subcircuit ensures high accuracy, the key objective for partitioning the subsequent subcircuits is for maximizing speedup. DCP equally partitions the remaining part of the quantum circuit into ‘ $k$ ’ subcircuits and assigns an equal arity to the rest of the subcircuits. In total DCP generates  $(k + 1)$  subcircuits. Since  $N = \prod_{j=0}^k A_j$ , we can calculate the number of shots allocated to each subcircuit by Equation 5 as described below:

$$A_1, \dots, A_k = A_r = \text{floor} \left( \sqrt[k]{\frac{N}{A_0}} \right) \quad (5)$$

If the calculated  $A_r$  for the rest of the subcircuits is less than 2, it means we do not reuse any of the intermediate states. Thus, for optimal speedup, TQSim selects the maximum number of subcircuits (the maximum value of ‘ $k$ ’) such that  $A_r \geq 2$ . It then adjusts the generated uniform sequence, by adding





(a) Bernstein-Vazirani circuit partitioned into three subcircuits. Each subcircuit is indicated by a coloured circle.

(b) Simulation tree of the baseline simulator. The tree structure is represented as (64,1,1).

Fig. 7: Graphical representation of the Bernstein-Vazirani circuit and the baseline simulation tree. The baseline simulation tree has 193 nodes – 192 subcircuit nodes and 1 initial state node. The baseline simulation produces 64 outcomes.

one to each individual shot starting from the first subcircuit. This ensures that TQSim always produces *at least* the user-specified number of outcomes. Figure 8 shows a simulation tree of the 3-qubit Bernstein-Vazirani circuit with three TQSim generated subcircuits.

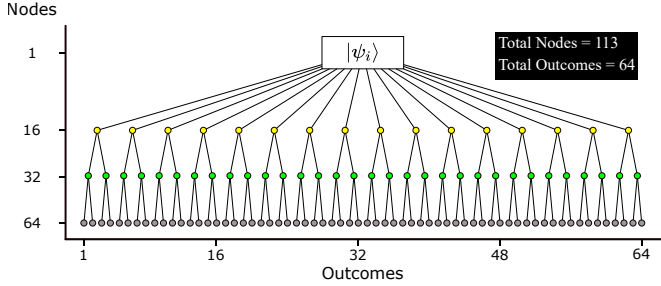


Fig. 8: Simulation tree of TQSim using Dynamic Circuit Partition (DCP). The TQSim structure is (16,2,2). The simulation tree has 113 nodes and produces 64 outcomes.

### C. Tradeoff: Number of Subcircuits vs State-Copy Overhead

The number of subcircuits determines the upper bound on the achievable speedup. For example, with two equal length subcircuits, one can obtain a maximum speedup with a TQSim structure of (1, N). The corresponding maximum speedup is  $\frac{1+N}{2N} \approx 1.5\times$  and ignores the accuracy measure. On the other hand, we can easily achieve a similar speedup with a higher accuracy using more subcircuits.

The maximum speedup with ‘k’ equal-length subcircuits is  $\frac{(k-1)+N}{kN}$  where ‘N’ is the number of shots. We can see that the maximum speedup increases as ‘k’ increases. Therefore, a higher number of subcircuits results in a potentially higher speedup. However, we cannot naively increase the number of subcircuits as each additional subcircuit imposes a memory overhead (for storing the state) and execution overhead (for copying the state). To address the memory overhead constraint, we set the maximum number of subcircuits such that their size does not exceed the current memory capacity limit. To address the execution time overhead, we profile the state-copy cost, using a set of profiling circuits, and normalize it to the execution time of one gate. We use the state-copy cost to select the maximum number of subcircuits.

Figure 9 shows the state copy cost normalized to the execution time of one gate on the same machine for 6 systems. For example, when doing a simulation on a desktop GPU, the time it takes to copy a state is approximately the execution time of 10 gates. We observe that for circuits with different numbers of qubits, the state copy cost is close. Therefore, we use an averaged state copy cost value for all circuit widths. We set the minimum number of gates in a subcircuit to be equal to state copy cost. This way, the state copy overhead does not dominate the execution time. With this minimum number of gates limit, we effectively set the maximum number of subcircuits for a simulation task.

We see that the state copy cost is much higher on server CPU systems. This is because we normalize the state copy time to the execution time of one gate on the same machine. The server memories are running at  $1.2\times$  lower frequency as compared to desktop memories – DDR4-3200 vs DDR4-2666 respectively. Therefore, it takes longer to copy a state on server systems. On the other hand, server systems have more high-performance cores as compared to desktop systems. Thus, server systems have a big compute advantage over desktop systems. This results in that server systems taking much less time to *execute* a gate. These two combined factors result in a much higher normalized state copy cost for server systems. Contrary to CPUs, the NVIDIA® Tesla® V100 system uses a faster HBM2 memory system and thus its state copy cost is also the lowest.

The final maximum number of subcircuits will be the minimum of the two limits we calculated with memory constraint and execution constraint.

### D. Individual Qubit Error Rates

An important factor that affects the output accuracy is the individual qubit error frequency. We use a 12-qubit Quantum Fourier Transform (QFT) circuit to illustrate the result. The initial state we use for the QFT\_12 circuit is the equal superposition state. The resulting state for QFT\_12, therefore, should be  $|0\rangle^{\otimes 12}$ . Therefore, any measurement of  $|1\rangle$  state from a qubit indicates a qubit error.

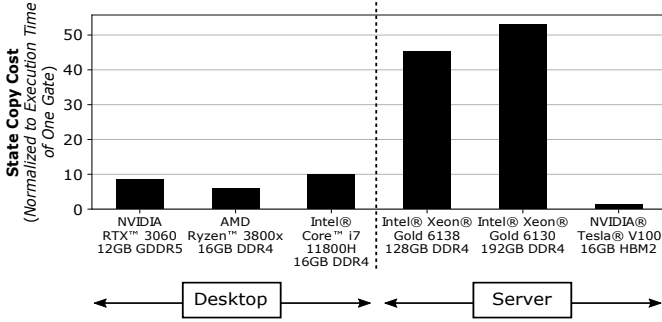


Fig. 9: The state copy overhead across different systems. The cost of copying a Statevector is normalized to the execution time of one gate on the same machine. A state copy cost of 20 gates indicates that the time to copy a Statevector is equal to the execution time of 20 gate operations.

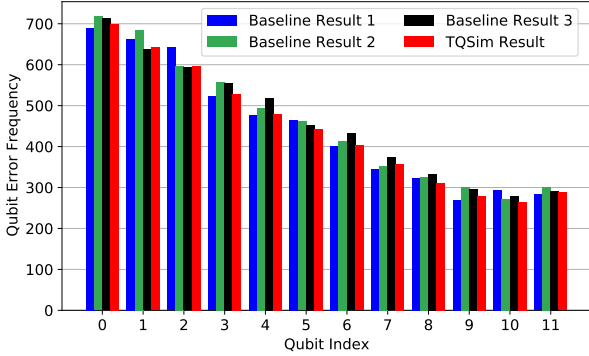


Fig. 10: Qubit error frequencies of three baseline results - running baseline simulator three times, and one TQSim result of the QFT<sub>12</sub> circuit. The initial state is set to be the equal superposition state. The ideal simulation should output a state of  $|0\rangle^{\otimes 12}$ . Any measurement of  $|1\rangle$  state indicates a qubit error.

Figure 10 shows the qubit error frequency of three baseline results and the TQSim result. The individual error frequency for each qubit is consistent across all three baseline results. The TQSim result is closely matched with baseline results across all the qubits<sup>2</sup> and is interchangeable with the baseline results. This high accuracy behaviour of TQSim is *not* specifically tied to the special output distribution of the QFT<sub>12</sub> circuit. In general, TQSim consistently provides very high accuracy across a range of circuits. Section V provides a more in-depth accuracy analysis.

#### IV. METHODOLOGY

##### A. Figure of Merit

State fidelity is used as a metric to measure the similarity between two quantum states. We use Equation 6 and Equation 7, as defined by Lubinski et. al. [30], to compute the state fidelity for noisy simulations. State fidelity is evaluated by computing the inner product of the qubit Statevectors between ideal and noisy results. For identical quantum states,

<sup>2</sup>Note that two noise operators may cancel with each other which leaves with a correct state, but this scenario can happen in both simulators, therefore, this does not overturn the conclusion made from this experiment.

the fidelity is one, whereas fidelity is zero for two completely different (orthogonal) states.

$$F_s(P_{\text{ideal}}, P_{\text{output}}) = \left( \sum_x \sqrt{P_{\text{ideal}}(x)P_{\text{output}}(x)} \right)^2 \quad (6)$$

One problem with the fidelity metric is that  $F_s$  is not 0 when the output is completely random, i.e. the  $P_{\text{output}}$  is uniform. To address this, we use the normalized fidelity metric, as defined by Hashim et. al. [20] and Lubinski et. al. [30], as shown below:

$$F(P_{\text{ideal}}, P_{\text{output}}) = \frac{F_s(P_{\text{ideal}}, P_{\text{output}}) - F_s(P_{\text{ideal}}, P_{\text{uni}})}{1 - F_s(P_{\text{ideal}}, P_{\text{uni}})} \quad (7)$$

For quantum simulators that *do not* model noise, we can evaluate the accuracy of a framework by first running the circuit on an ideal reference simulator and then running the same circuit on the proposed simulator, and computing their output similarity. This methodology is used by several prior works [42], [46]. Unfortunately, to quantify the accuracy of TQSim, we can not directly use normalized fidelity. This is because TQSim is designed to accelerate noisy quantum circuit simulations. Even on the baseline simulator, we may not get identical output distributions with the same ‘N’ shots due to the probabilistic nature of noise. Therefore, for a fair comparison, we first calculate a reference normalized fidelity using the baseline simulator and compare it with the normalized fidelity of TQSim. Closely matched normalized fidelity values show the baseline result and TQSim result are interchangeable.

##### B. Benchmarks

We use quantum circuits with 6 to 25 qubits from Qasm-Bench, Qiskit, Cirq, and Qualcs [10], [12], [24], [41]. We use arithmetic quantum circuits such as Adders, Multipliers, Quantum Fourier Transform (QFT), Quantum Phase Estimation (QPE). These circuits are used as subroutines for factorization, chemistry simulation, and quantum search algorithms. Table I summarizes key parameters for these circuits such as the number of qubits and gate counts. Moreover, we use near-term quantum algorithms such as Quantum Approximate Optimization Algorithm (QAOA) and Bernstein Vazirani (BV) [5], [15]. These algorithms can be run on existing noisy quantum computers [9], [22].

To rigorously evaluate the accuracy and speedup of TQSim, we use Quantum Supremacy (QSC) and Quantum Volume (QV) circuits. These circuits are non-trivial to simulate due to lack of structure. QSC and QV circuits are also used to benchmark quantum hardware. For example, to compute the Quantum Volume, QV circuits are run on both the simulator and the real hardware wherein output from a simulator is used as a reference. Unfortunately, with increasing qubits, noisy QV simulations require exponentially longer time compared to ideal simulations. TQSim can help speed up such noisy simulations.

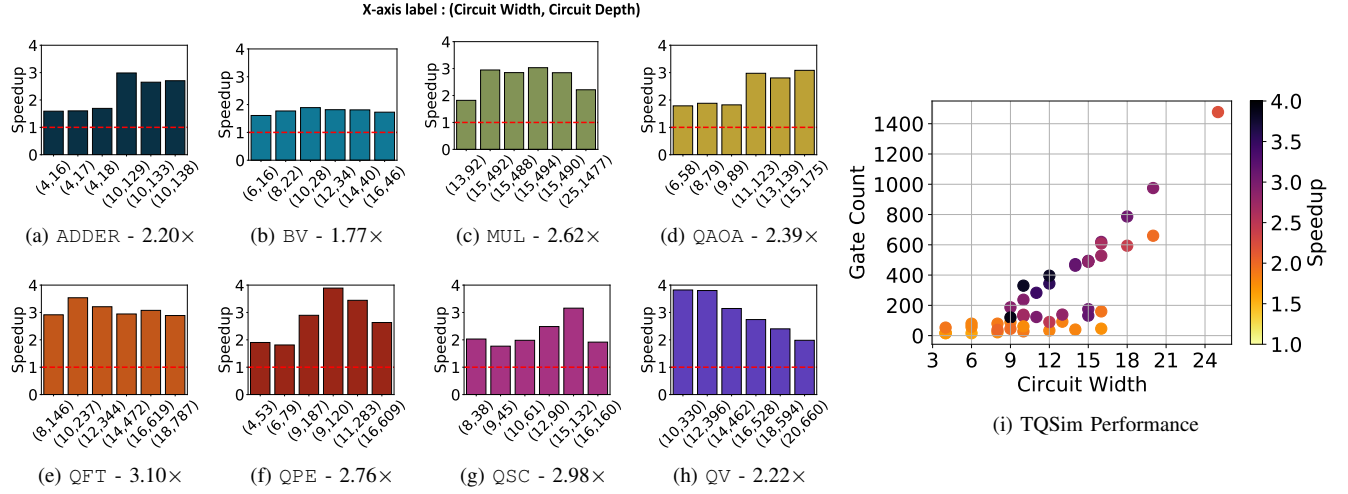


Fig. 11: Speedups of TQSim over the baseline simulator for 8 benchmark circuits. The tuple indicates the width and length of the circuit. For example, the first ADDER circuit in (a) has 4 qubits and 16 gates. The experiments are running on two 16-core Intel® Xeon® 6130 processors.

TABLE I: Benchmark Characteristics

Benchmark	Description	Width	Gate Counts
ADDER	Quantum Adder [10], [24]	4-10	16-133
BV	Bernstein-Vazirani [5], [10]	6-16	16-46
MUL	Quantum Multiplier [10]	13-25	92-1477
QAOA	Quantum Approx. Optimization Algorithm [15]	6-15	58-175
QFT	Quantum Fourier Transform [10]	10-20	237-975
QPE	Quantum Phase Estimation [10], [24]	4-16	53-609
QSC	Quantum Supremacy Circuit [2], [12]	8-16	38-160
QV	Quantum Volume [11], [41]	10-20	330-660

### C. Simulation Parameters

1) *Number of Shots*: For speedup tests, we use 32,000 shots across benchmarks. We ensure that the number of shots is sufficient for the noisy quantum circuits with 6 to 25 qubits used in our evaluations. Additionally, we perform sensitivity tests that vary the number of shots and examine the accuracy and speedups of TQSim. For the two sensitivity tests on the accuracy, we reduce the number of shots to 1000 and 3200 respectively to amplify the effect of noise.

2) *Noise Models*: We use depolarizing noise model to highlight the benefits of TQSim. Additionally, for sensitivity studies, we select a set of circuits that have different characteristics to verify the accuracy of TQSim with an exhaustive set of noise models that are constructed using error channels including: *thermal relaxation*, *amplitude damping*, *phase damping*, and *readout error*:

- 1) **Depolarizing Channel (DC)**: Uses Pauli operators (I, X, Y, Z) to model errors.
- 2) **Thermal Relaxation Channel (TR)**: Models the decoherence of the qubit system. The channel is constructed using the T1, T2 and gate time of a quantum computer.
- 3) **Amplitude Damping (AD)**: Models energy relaxation of the qubit systems through a set of Kraus operators. In our

test, we use a damping ratio of 0.01.

- 4) **Phase Damping (PD)**: Phase damping channel also uses a set of Kraus operators to model phase damping noise. We use a damping ratio of 0.01.

- 5) **Readout Error (RE)**: During measurement, a measured classical bit is been flipped with a given probability.

The characteristics of the noise models we use for the sensitivity studies are listed in Table II.

TABLE II: Noise Model Characteristics

Name	Error Channel(s)
DC	Depolarizing Channel
DCR	DC with Readout Error
TR	Thermal Relaxation Channel
TRR	TR with Readout Error
AD	Amplitude Damping Channel
ADR	AD with Readout Error
PD	Phase Damping Channel
PDR	PD with Readout Error
ALL	All Channels Combined

- 3) *Error Rate*: Our evaluations use realistic device error rates obtained from Google Sycamore [1], [2]. For error channels that don't have profiled parameters from actual devices, we select the error parameters that cause a large noise effect on the result. For example, we use a damping ratio of 0.01 for both amplitude and phase damping channels. This is because a larger damping ratio will force the resulting state to be relaxed to the ground state and a smaller damping ratio have a negligible effect on the result.

### D. System Configuration

We evaluate TQSim simulator on a platform with two Intel® Xeon® Gold 6130 processors @ 2.10 GHz, each has 16 physical cores with 192GB DDR4-2666 memory. We also evaluate the performance of TQSim design on a GPU-driven simulation setup using NVIDIA® V100 card with 16 GB of VRAM. Both baseline and TQSim use all compute cores and threads in CPU and GPU respectively.

## V. EVALUATION

We use *Qulacs* [41] as our baseline noisy quantum circuit simulator<sup>3</sup>.

### A. TQSim: Performance

Figure 11 shows the performance of TQSim over the baseline *Qulacs* simulator for all the benchmark circuits. Overall, TQSim is  $1.59\times$  to  $3.89\times$  faster compared to baseline simulator and on average it provides  $2.51\times$  speedup. In general, the circuits with small width and depth, such as ADDER circuits, have the least room for improvement as we can not partition them into a large number of subcircuits. TQSim still achieves  $2.2\times$  speedup for such circuits.

With increasing circuit depth and gate count, we can increase the number of subcircuits to enable higher speedup. However, to maintain a high simulation accuracy for the realistic error rates, TQSim limits the maximum number of subcircuits. For example, to simulate QFT\_14 that has 472 gates with a 0.1% gate error rate, TQSim partitions the input circuit into seven subcircuits and assigns 500 shots to the first subcircuit. This results in a theoretical maximum speedup of  $3.53\times$ . As shown in Figure 11e, TQSim provides  $3.21\times$  speedup for QFT\_14, which is close to the theoretical maximum speedup. This indicates that the benefits of circuit partition and state reuse are higher than the overhead in creating copies for subcircuits.

The circuits with large width and small depth can not be partitioned into multiple subcircuits. Also, the intermediate state transfer overhead for the high width subcircuit is significantly higher than circuits with a smaller width. These two factors result in lower speedups for such benchmarks. For example, the BV circuits in Figure 11b can only be partitioned into 2 subcircuits. They show a speedup of  $1.61\times$ - $1.89\times$ . Table III shows the simulation time of three medium-scale circuits (18-20 qubits).

TABLE III: Simulation Time: Medium-Scale Circuits

Benchmark	Baseline Simulation Time (min)	TQSim Simulation Time (min)	Speedup
QV_18	23.5	9.7	$2.43\times$
QV_20	55.4	36.6	$2.03\times$
QFT_20	46.4	16.1	$2.88\times$

Figure 11i summarizes the speedups with respect to both the circuit width and the gate count. From Figure 11i, we observe that the main challenge of TQSim simulator is the relatively low speedups for circuits with high width and low depth, i.e. square circuits. However, square circuits have high fidelity on NISQ hardware. The real challenge is when we want to study how noise impacts the fidelity of circuits with higher depth. Circuits with large depth are significantly more prone

<sup>3</sup>The ideas on computation reuse that are proposed in the paper are focused on optimizing simulation time and accuracy in the presence of noise. Thus, they are independent of the choice of the underlying ideal simulator. The user will continue to experience the benefits of TQSim even if they replace *Qulacs* [41] with any other simulator.

to errors and noise, studying the effect of noise methodically becomes hard. Simulating quantum circuits with parametric noise can help us better understand the impact of noise on fidelity. Unfortunately, simulating high-depth circuits on a conventional quantum simulator is slow. For example, the baseline simulator takes around 46 minutes to simulate a medium-size 20-qubit QFT circuit for 32,000 shots, whereas TQSim solves this problem  $2.88\times$  faster compared to baseline simulations.

### B. TQSim: Outcome Accuracy as Compared to Baseline

Figure 12 shows the differences between baseline normalized fidelity and TQSim normalized fidelity. For all benchmarks, we observe a difference of normalized fidelity values less than 0.016. The benchmark circuits cover a wide range of circuit width, length, and types of output distributions. Thus, with a fixed number of shots, we observe a wide range of baseline normalized fidelity. Still, TQSim manages to provide a result with a normalized fidelity that is within 0.016 range of the baseline normalized fidelity. We provide a more in-depth analysis of the accuracy of the TQSim as compared to baseline results in Section V-E

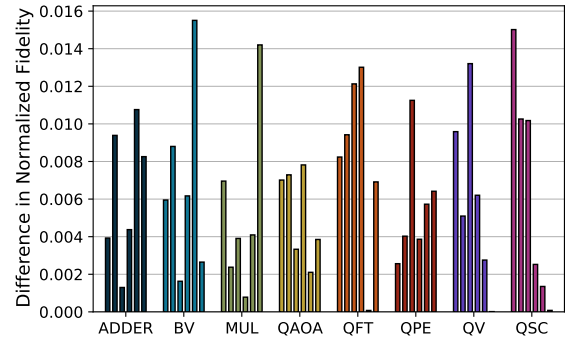


Fig. 12: Baseline and TQSim normalized fidelity difference across 48 benchmarks. The average and maximum difference is only 0.006 and 0.016 (negligible) respectively.

### C. Tradeoff: Outcome Accuracy versus Speedup

We examine the relation between speedup and the accuracy of the output distribution. To that end, we use a 9-qubit QPE circuit that has 120 gates as it is sensitive to the TQSim structure. Furthermore, we lower the total number of shots to 1000 to amplify the difference between baseline and TQSim in the output distributions. DCP generates one TQSim structure. Beyond that, we have manually created four additional TQSim structures that have a higher speedup potential but sacrifice accuracy. Thus, in total, we compare five TQSim structures with the baseline simulator. All the TQSim structures are having the same circuit partition but different shot allocations. Table IV shows the five TQSim structures and their maximum possible speedups. The maximum possible speedups for each TQSim structure is estimated by calculating the node ratios between its TQSim and baseline simulation tree.

For accuracy purposes, we repeat the same experiment 10 times and take the mean normalized fidelity value. Figure 13



TABLE IV: Speedup of QPE at lower shots.

TQSim Structure	Maximum Speedup
(250,2,2)	1.71×
(20,10,5)	2.46×
(10,10,10)	2.70×
(5,10,20)	2.84×
(2,2,250)	2.98×

shows the speedups and the mean normalized fidelity differences for each TQSim structure. TQSim can produce a highly accurate result with up to 2.52× speedup. Beyond that, a small increment in speedup causes a large drop in accuracy.

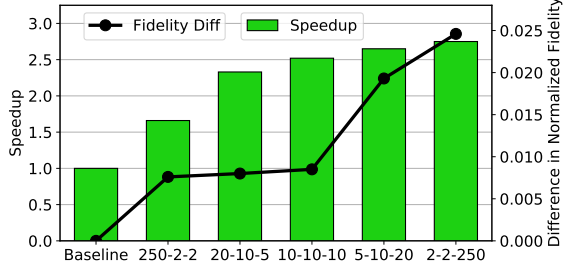
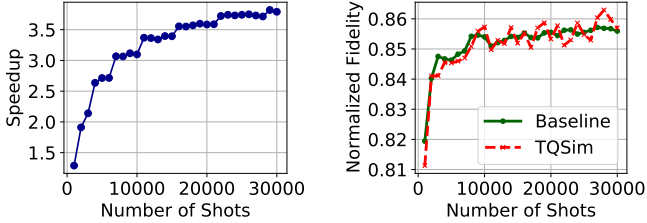


Fig. 13: Speedups and difference in normalized fidelity for QPE\_9 using 5 TQSim structures as compared to baseline simulator while executing on two 16-core Intel® Xeon® 6130 processors.

#### D. Sensitivity: Varying Number of Shots

The total number of shots is an important factor for circuit partition. We present a sensitivity test with QPE\_9 circuit using 1000 to 32000 shots. For accuracy measure, we repeat each experiment 10 times and report the mean speedup value and normalized fidelity.



(a) Speedup of TQSim as the number of shots varies. (b) Baseline normalized fidelity and TQSim normalized fidelity for a different number of shots.

Fig. 14: Impact on speedup and accuracy of TQSim when varying the number of shots. These experiments are running on two 16-core Intel® Xeon® 6130 processors.

The total number of shots limits the height of the simulation tree and therefore limits the speedup. Figure 14a shows the speedups of TQSim with a different number of shots. The speedup increases from 1.3× to 3.1× as the total number of shots increases from 1,000 to 7,000. After that, the speedup value gradually saturates and eventually reaches 3.8× for 32,000 shots.

Figure 14b shows the normalized fidelity values for both baseline simulator and TQSim. The baseline normalized fidelity saturates at 0.85 from 9000 shots onward. The maximum

difference in normalized fidelity between baseline result and TQSim result is 0.008.

#### E. Sensitivity: Varying Noise Models

In this section, we select three circuits that have different characteristics and output distributions to analyze the accuracy of TQSim. For each experiment, we repeat the simulation 10 times and report the average normalized fidelity for both baseline result and TQSim result.

With the baseline simulator, we observe that the depolarizing channel has the largest effect on the accuracy measure, thus, we use the parameters from depolarizing channel to generate the TQSim structure and use it across all noise models experiments for each circuit.

1) *QFT\_12*: The 12-qubit QFT circuit outputs an equal superposition state when the input is  $|0\rangle^{\otimes 12}$  and outputs a  $|0\rangle^{\otimes 12}$  state when input is the equal superposition state. The initial state we use is  $|0\rangle^{\otimes 12}$  and we insert a set of Hadamard gates at the beginning of the circuit to make the output distribution in between of a uniform distribution and a distribution with a single possible output.

Figure 15a shows the accuracy results for QFT\_12. The QFT\_12 is not very prone to readout error as the error may convert a correct outcome to another correct outcome. However, its large gate count makes it sensitive to other error channels. With an all-combined noise model, the normalized fidelity dropped to 0.3 as compared to 0.9 when using the thermal relaxation channel. TQSim results are closely matched with baseline results for all noise models.

2) *QPE\_9*: The QPE circuit estimates the phase (eigenvalue) corresponding to an eigenvector of a unitary operator. The eigenvalue this 9-qubit QPE circuit estimates is  $\frac{1}{3}$  and cannot be exactly represented by a 9-bit fixed-point number. Thus, the output distribution is a narrow bell curve with high probability existing around fixed-point representations of the numbers that are closest to  $\frac{1}{3}$ .

Figure 15b shows the experimental results for QPE\_9. The ideal output distribution of QPE\_9 has fewer possible outcomes as compared to QFT\_12, thus, it is more prone to readout errors. QPE\_9 sensitive to DC, TR and AD due to its high gate count. This results in a very low normalized fidelity for QPE\_9 when using an all-combined noise model. In all cases, TQSim produces a closely matched result across noise models.

3) *BV\_10*: The 10-qubit BV Circuit has a single possible output which is the hidden string encoded in the oracle function. We set the hidden string to be all ones.

Figure 15c shows the accuracy results for BV\_10. Since the ideal output has a single possible output, the readout error channel has the largest effect across all three benchmark circuits selected. Due to its shallow circuit depth, the effects of other error channels are much smaller. Again, TQSim manages to produce a result that is closely matched with the baseline result for all noise models tested.

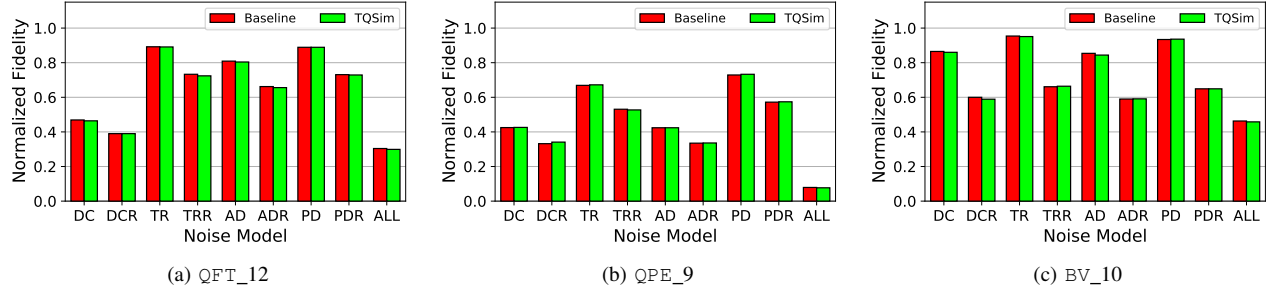


Fig. 15: Normalized fidelity values for three benchmark circuits executing with nine noise models. The error channels each noise model contains is listed in Table II. For circuits with different output distributions and executing with different noise models, TQSim manages to produce a closely matched results.

#### F. TQSim: GPU-based Quantum Circuit Simulation

Figure 16 shows the performance for TQSim running on GPU compared to baseline *Qulacs* simulator also running on the same GPU. Our evaluations show similar results as the CPU simulator. This is expected as TQSim does not alter the parallel structure of the original computation task. Current optimization techniques, such as multiprocessing and GPU acceleration, for quantum circuit simulations are for the single-shot simulation. Therefore, the only overhead added by TQSim on the GPU simulator is the communication overhead between GPU and TQSim scheduler. Our evaluation shows that the overheads are negligible compare to the overall simulation time.

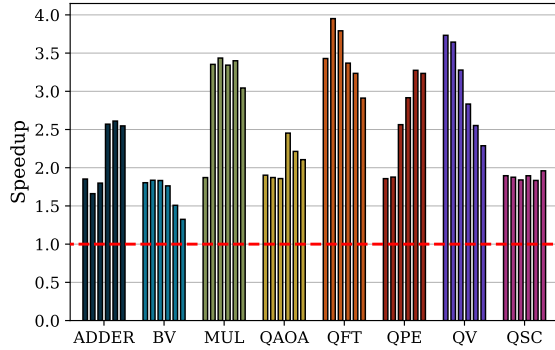


Fig. 16: The performance of TQSim-GPU as compared to Qulacs-GPU simulator for 48 benchmark circuits. The first six bars show the speedups for the six ADDER circuits, the rest of the bars can be interpreted in the same manner. The experiments are running on NVIDIA® Tesla® V100 GPU.

## VI. DISCUSSION

#### A. Limitations of TQSim

We observe a reduction in TQSim speedup for both CPU and GPU with an increasing number of qubits for benchmarks like BV and QV. For these circuits, the total number of gates scales linearly with the number of qubits. As a result, the size of quantum states scales exponentially faster compared to circuit partition opportunities. For such square-shaped circuits, beyond 35 qubits, the overhead of creating copies of intermediate state can outweigh the reduction in computation

enabled by TQSim. On the other hand, TQSim shows a significant speedup for key quantum circuits and subroutines such as QAOA, QFT, and QPE, wherein the total gates scale polynomially with qubits. Overall, TQSim can significantly enhance users' ability to analyze the impact of noise on key quantum benchmarks.

#### B. Case Study: Grid Search for QAOA Parameters

TQSim can enable significantly faster design cycles. To illustrate this, we use TQSim and baseline simulators to run QAOA circuits designed to solve the Max-Cut problem. In Max-Cut, we want to partition all nodes of an input graph into two sets that maximize the number of edges that connect vertices from different sets. Figure 17 shows the two graphs and the optimal partition we use in our study. To run QAOA we need an input graph and two circuit parameters: beta and gamma. The range for both beta and gamma is  $(0, \pi)$ . We use grid search with a step size of 0.1 to find the optimal beta and gamma that produces the optimal cut with a high probability. To search this parameter space, we need  $32 * 32 = 1024$  QAOA circuits for each graph.

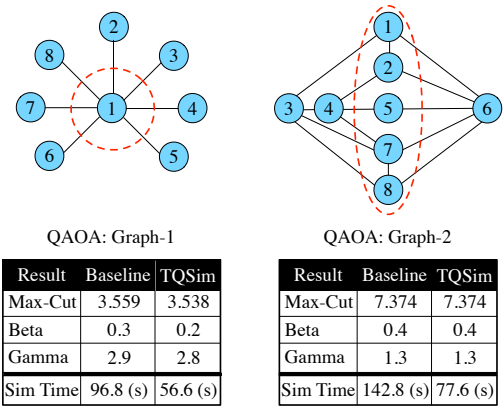


Fig. 17: Graphs for QAOA case study and their results.

The tables in Figure 17 show optimal beta and gamma obtained for two graphs with TQSim and baseline. The expected cost of Max-Cuts, beta, and gamma values from the baseline simulator and the TQSim simulator are almost identical for both graph 1 and graph 2.

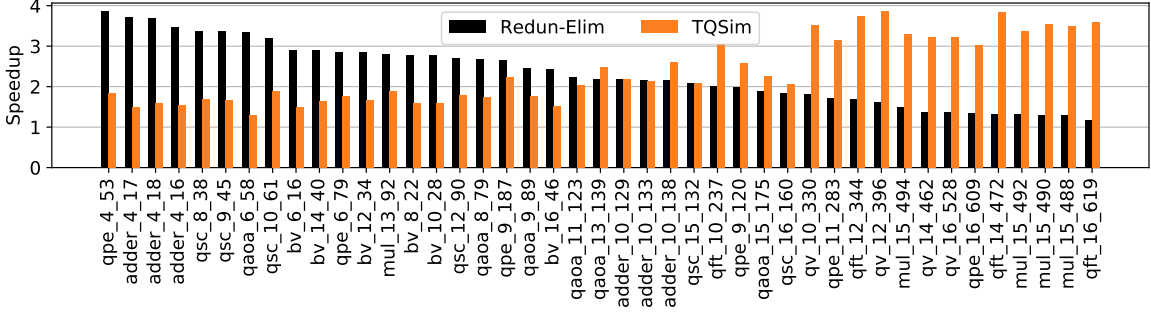


Fig. 18: Experiment results of redundancy elimination (Redun-Elim) method as compared to TQSim. Noise is modelled using the depolarizing channel. The x label shows the benchmark name, width, and the number of gates it contains. The experiments are running on two 16-core Intel® Xeon® 6130 processors.

## VII. RELATED WORK

Quantum simulators and software tools will play a vital role in designing, verifying, and tuning the quantum circuits [8], [31], [36]. For example, quantum compilers optimize circuits by reducing the number of gates and tailoring quantum executables to enhance the application fidelity [7], [26], [28], [32]–[34], [37], [39], [43], [49]. Moreover, recent works focus on architecture and runtime systems for quantum architectures [3], [13], [14], [21], [25], [28]. The simulations tools, especially noise simulators, would be even more important in the future. This is because researchers will need to understand the impact of noise on different algorithms, compilers and architectures.

### A. Ideal Simulation Optimization

Prior work HyQuas [48] for example, partitions the quantum circuit into multiple subcircuits by its depth and uses different simulation techniques for each subcircuit to enable speedup for ideal simulation. CutQC [42], on the other hand, partitions the quantum circuit into subcircuits along its width such that each subcircuit requires fewer qubits and can be executed on a smaller quantum computer and can be post-processed to generate complete output.

A recent work reduces the time for quantum circuit simulation by using gate fusion, data-level and thread-level parallelism, and improving cache utilization [16], whereas qHiPSTER [40], is a distributed quantum circuit simulator that can leverage multi-node HPC clusters. Many works focus on reducing the memory requirement of quantum simulation by using knowledge graphs, decision trees, and data compression [22], [44], [46]. Moreover, a class of quantum circuit simulators can simulate special quantum circuits efficiently [6], [17], [45].

Prior works on simulation methods primarily focus on ideal quantum circuits that sample from a single probability distribution [16], [40], [42], [48]. TQSim can be combined with techniques proposed to improve single-shot simulation time to achieve an even better simulation result.

### B. Inter-Shot Noisy Simulation Optimization

Li et. al [27] proposed an inter-shots redundancy elimination technique. It searches, among all the noisy-version circuits,

for the identical circuit portions and preserves intermediate states to save computation for those redundancies. Since the targets of elimination are identical computations, the accuracy of the final result is not affected. The experiment results show the redundancy elimination method can eliminate up to 90% or more computations for a small to medium scale circuit. However, the ratio of absolute redundancy drops as the gate count in the circuit increases. Under the current error rates that are profiled from Google’s Sycamore Quantum Computer, the ratio of redundancy drops to near zero as the gate count exceeds 200. The differences between the two methods are summarized in this section as follows:

1) *Pre-processing overhead*: The redundancy elimination method requires first generating all the noisy circuits and then searching for the common pattern among them. This introduces both memory overhead for storing the noisy circuits and execution overhead for searching.

2) *Scalability*: Both TQSim and redundancy elimination methods face scalability issues. In both methods, the available memory limits the number of additional states that can be preserved and any additional intermediate state also introduces state copy overhead. Beyond this, the scalability of the Redundancy Elimination Method is also limited by the length of the circuit. As the number of gate increases in the circuit, the proportion of the circuit that has consecutive identical gates decreases. As a result, the ratio of absolute identical subcircuits across shots decreases.

3) *Experimental Results*: Figure 18 shows the experiment results of the redundancy elimination method applied to the benchmarks used in this paper. For circuits with less than 150 gates, the redundancy elimination method performs very well and can have up to  $2\times$  the speedup as compared to TQSim. However, as the gate count further increases, the speedup of the redundancy elimination method drops below TQSim and stays close to 1.

## VIII. CONCLUSION

Noisy quantum circuit simulators help the development of new algorithms and enable rapid design space exploration in the NISQ-era. Unfortunately, noisy quantum simulators iteratively execute noisy versions of the same circuit across

multiple shots and can incur up to  $100\times$  higher performance overheads as compared to ideal simulation.

To address this, we propose TQSim, a simulator that leverages computational reuse by using some intermediate results across multiple shots in a noisy quantum circuit simulation task. To enable this, TQSim dynamically partitions the sub-circuits and proposes an efficient shot-allocation method. We develop TQSim to execute on CPUs and GPUs. Overall, our experiments show that TQSim achieves an average of  $2.51\times$  speedup over existing noisy simulators while producing a result with a normalized fidelity that is within 0.016 range of baseline result.

## REFERENCES

- [1] G. Q. AI, “Quantum Computer Datasheet,” <https://quantumai.google/hardware/datasheet/weber.pdf>, 2021, [Online; accessed 1-July-2021].
- [2] F. Arute, K. Arya, R. Babbush, D. Bacon, J. Bardin, R. Barends *et al.*, “Quantum supremacy using a programmable superconducting processor,” p. 505–510, 2019. [Online]. Available: <https://www.nature.com/articles/s41586-019-1666-5>
- [3] J. M. Baker, A. Litteken, C. Duckering, H. Hoffmann, H. Bernien, and F. T. Chong, “Exploiting long-distance interactions and tolerating atom loss in neutral atom quantum architectures,” in *2021 ACM/IEEE 48th Annual International Symposium on Computer Architecture (ISCA)*. IEEE, 2021, pp. 818–831.
- [4] A. Bassi and D.-A. Deckert, “Noise gates for decoherent quantum circuits,” *Physical Review A*, vol. 77, no. 3, Mar 2008. [Online]. Available: <http://dx.doi.org/10.1103/PhysRevA.77.032323>
- [5] E. Bernstein and U. Vazirani, “Quantum complexity theory,” *SIAM Journal on computing*, vol. 26, no. 5, pp. 1411–1473, 1997.
- [6] S. Bravyi, D. Browne, P. Calpin, E. Campbell, D. Gosset, and M. Howard, “Simulation of quantum circuits by low-rank stabilizer decompositions,” *Quantum*, vol. 3, p. 181, Sep 2019. [Online]. Available: <http://dx.doi.org/10.22331/q-2019-09-02-181>
- [7] J. Cheng, H. Deng, and X. Qia, “Accqoc: Accelerating quantum optimal control based pulse generation,” in *2020 ACM/IEEE 47th Annual International Symposium on Computer Architecture (ISCA)*. IEEE, 2020, pp. 543–555.
- [8] F. T. Chong, D. Franklin, and M. Martonosi, “Programming languages and compiler design for realistic quantum hardware,” *Nature*, vol. 549, no. 7671, p. 180, 2017.
- [9] G. E. Crooks, “Performance of the quantum approximate optimization algorithm on the maximum cut problem,” *arXiv preprint arXiv:1811.08419*, 2018.
- [10] A. Cross, “The ibm q experience and qiskit open-source quantum computing software,” in *APS Meeting Abstracts*, 2018.
- [11] A. W. Cross, L. S. Bishop, S. Sheldon, P. D. Nation, and J. M. Gambetta, “Validating quantum computers using randomized model circuits,” *Physical Review A*, vol. 100, no. 3, Sep 2019. [Online]. Available: <http://dx.doi.org/10.1103/PhysRevA.100.032328>
- [12] C. Developers, “quantumlib/cirq: Cirq v0.9.1,” Oct. 2020, See full list of authors on Github: <https://github.com/quantumlib/Cirq/graphs/contributors>. [Online]. Available: <https://doi.org/10.5281/zenodo.4064322>
- [13] Y. Ding, A. Holmes, A. Javadi-Abhari, D. Franklin, M. Martonosi, and F. Chong, “Magic-state functional units: Mapping and scheduling multi-level distillation circuits for fault-tolerant quantum architectures,” in *2018 51st Annual IEEE/ACM International Symposium on Microarchitecture (MICRO)*. IEEE, 2018, pp. 828–840.
- [14] Y. Ding, X.-C. Wu, A. Holmes, A. Wiseth, D. Franklin, M. Martonosi, and F. T. Chong, “Square: strategic quantum ancilla reuse for modular quantum programs via cost-effective uncomputation,” in *2020 ACM/IEEE 47th Annual International Symposium on Computer Architecture (ISCA)*. IEEE, 2020, pp. 570–583.
- [15] E. Farhi, J. Goldstone, and S. Gutmann, “A quantum approximate optimization algorithm,” *arXiv preprint arXiv:1411.4028*, 2014.
- [16] A. Fatima and I. L. Markov, “Faster schrödinger-style simulation of quantum circuits,” in *IEEE International Symposium on High-Performance Computer Architecture, HPCA 2021, Seoul, South Korea, February 27 - March 3, 2021*. IEEE, 2021, pp. 194–207. [Online]. Available: <https://doi.org/10.1109/HPCA51647.2021.00026>
- [17] H. J. García and I. L. Markov, “Simulation of quantum circuits via stabilizer frames,” 2017.
- [18] L. K. Grover, “A fast quantum mechanical algorithm for database search,” *arXiv preprint quant-ph/9605043*, 1996.
- [19] G. G. Guerreschi and A. Y. Matsuura, “Qaoa for max-cut requires hundreds of qubits for quantum speed-up,” *Scientific Reports*, vol. 9, no. 1, May 2019. [Online]. Available: <http://dx.doi.org/10.1038/s41598-019-43176-9>
- [20] A. Hashim, R. K. Naik, A. Morvan, J.-L. Ville, B. Mitchell, J. M. Kreikebaum, M. Davis, E. Smith, C. Iancu, K. P. O’Brien *et al.*, “Randomized compiling for scalable quantum computing on a noisy superconducting quantum processor,” *arXiv preprint arXiv:2010.00215*, 2020.
- [21] A. Holmes, M. R. Jorak, G. Pasandi, Y. Ding, M. Pedram, and F. T. Chong, “Nisq+: Boosting quantum computing power by approximating quantum error correction,” in *2020 ACM/IEEE 47th Annual International Symposium on Computer Architecture (ISCA)*. IEEE, 2020, pp. 556–569.
- [22] Y. Huang, S. Holtzen, T. Millstein, G. Van den Broeck, and M. Martonosi, “Logical abstractions for noisy variational quantum algorithm simulation,” in *Proceedings of the 26th ACM International Conference on Architectural Support for Programming Languages and Operating Systems*, ser. ASPLOS 2021. New York, NY, USA: Association for Computing Machinery, 2021, p. 456–472. [Online]. Available: <https://doi.org/10.1145/3445814.3446750>
- [23] IBM, “Quantum Computing Systems,” <https://www.ibm.com/quantum-computing/systems/>, 2021, [Online; accessed 18-Nov-2021].
- [24] A. Li, S. Stein, S. Krishnamoorthy, and J. Ang, “Qasmbench: A low-level qasm benchmark suite for nisq evaluation and simulation,” 2021.
- [25] G. Li, Y. Shi, and A. Javadi-Abhari, “Software-hardware co-optimization for computational chemistry on superconducting quantum processors,” in *2021 ACM/IEEE 48th Annual International Symposium on Computer Architecture (ISCA)*, 2021.
- [26] G. Li, Y. Ding, and Y. Xie, “Tackling the qubit mapping problem for nisq-era quantum devices,” *arXiv preprint arXiv:1809.02573*, 2018.
- [27] G. Li, Y. Ding, and Y. Xie, “Eliminating redundant computation in noisy quantum computing simulation,” in *2020 57th ACM/IEEE Design Automation Conference (DAC)*, 2020, pp. 1–6.
- [28] G. Li, Y. Ding, and Y. Xie, “Towards efficient superconducting quantum processor architecture design,” in *Proceedings of the Twenty-Fifth International Conference on Architectural Support for Programming Languages and Operating Systems*, 2020, pp. 1031–1045.
- [29] S. Lloyd, “Universal quantum simulators,” *Science*, pp. 1073–1078, 1996.
- [30] T. Lubinski, S. Johri, P. Varosy, J. Coleman, L. Zhao, J. Necaie, C. H. Baldwin, K. Mayer, and T. Proctor, “Application-oriented performance benchmarks for quantum computing,” 2021.
- [31] M. Martonosi and M. Roetteler, “Next steps in quantum computing: Computer science’s role,” *arXiv preprint arXiv:1903.10541*, 2019.
- [32] P. Murali, J. M. Baker, A. J. Abhari, F. T. Chong, and M. Martonosi, “Noise-adaptive compiler mappings for noisy intermediate-scale quantum computers,” *arXiv preprint arXiv:1901.11054*, 2019.
- [33] P. Murali, N. M. Linke, M. Martonosi, A. J. Abhari, N. H. Nguyen, and C. H. Alderete, “Full-stack, real-system quantum computer studies: architectural comparisons and design insights,” in *Proceedings of the 46th International Symposium on Computer Architecture*, 2019, pp. 527–540.
- [34] P. Murali, D. C. McKay, M. Martonosi, and A. Javadi-Abhari, “Software mitigation of crosstalk on noisy intermediate-scale quantum computers,” *arXiv preprint arXiv:2001.02826*, 2020.
- [35] M. Noordzij, G. Tripepi, F. W. Dekker, C. Zoccali, M. W. Tanck, and K. J. Jager, “Sample size calculations: basic principles and common pitfalls,” *Nephrology Dialysis Transplantation*, vol. 25, no. 5, pp. 1388–1393, 01 2010.
- [36] N. A. of Sciences Engineering and Medicine, *Quantum Computing: Progress and Prospects*, E. Grumbling and M. Horowitz, Eds. Washington, DC: The National Academies Press, 2019. [Online]. Available: <https://www.nap.edu/catalog/25196/quantum-computing-progress-and-prospects>
- [37] T. Patel and D. Tiwari, “Qraft: reverse your quantum circuit and know the correct program output,” in *Proceedings of the 26th ACM International Conference on Architectural Support for Programming Languages and Operating Systems*, 2021, pp. 443–455.



- [38] P. W. Shor, "Polynomial-time algorithms for prime factorization and discrete logarithms on a quantum computer," *SIAM review*, vol. 41, no. 2, pp. 303–332, 1999.
- [39] M. Siraichi, V. F. Dos Santos, S. Collange, and F. M. Q. Pereira, "Qubit allocation," in *CGO 2018-IEEE/ACM International Symposium on Code Generation and Optimization*, 2018, pp. 1–12.
- [40] M. Smelyanskiy, N. P. D. Sawaya, and A. Aspuru-Guzik, "qhipster: The quantum high performance software testing environment," 2016.
- [41] Y. Suzuki, Y. Kawase, Y. Masumura, Y. Hiraga, M. Nakadai, J. Chen, K. M. Nakanishi, K. Mitarai, R. Imai, S. Tamiya, T. Yamamoto, T. Yan, T. Kawakubo, Y. O. Nakagawa, Y. Ibe, Y. Zhang, H. Yamashita, H. Yoshimura, A. Hayashi, and K. Fujii, "Qulacs: a fast and versatile quantum circuit simulator for research purpose," 2020.
- [42] W. Tang, T. Tomesh, M. Suchara, J. Larson, and M. Martonosi, "Cutqc: Using small quantum computers for large quantum circuit evaluations," in *Proceedings of the 26th ACM International Conference on Architectural Support for Programming Languages and Operating Systems*, ser. ASPLOS 2021. New York, NY, USA: Association for Computing Machinery, 2021, p. 473–486. [Online]. Available: <https://doi.org/10.1145/3445814.3446758>
- [43] S. S. Tannu and M. K. Qureshi, "Mitigating measurement errors in quantum computers by exploiting state-dependent bias," in *Proceedings of the 52nd Annual IEEE/ACM International Symposium on Microarchitecture*, 2019, pp. 279–290.
- [44] G. Viamontes, I. Markov, and J. Hayes, "High-performance quidd-based simulation of quantum circuits," in *Proceedings Design, Automation and Test in Europe Conference and Exhibition*, vol. 2, 2004, pp. 1354–1355 Vol.2.
- [45] G. Vidal, "Efficient classical simulation of slightly entangled quantum computations," *Physical Review Letters*, vol. 91, no. 14, Oct 2003. [Online]. Available: <http://dx.doi.org/10.1103/PhysRevLett.91.147902>
- [46] X.-C. Wu, S. Di, E. M. Dasgupta, F. Cappello, H. Finkel, Y. Alexeev, and F. T. Chong, "Full-state quantum circuit simulation by using data compression," in *Proceedings of the International Conference for High Performance Computing, Networking, Storage and Analysis*, ser. SC '19. New York, NY, USA: Association for Computing Machinery, 2019. [Online]. Available: <https://doi.org/10.1145/3295500.3356155>
- [47] Y. Wu, W.-S. Bao, S. Cao, F. Chen, M.-C. Chen, X. Chen, T.-H. Chung, H. Deng, Y. Du, D. Fan, M. Gong, C. Guo, C. Guo, S. Guo, L. Han, L. Hong, H.-L. Huang, Y.-H. Huo, L. Li, N. Li, S. Li, Y. Li, F. Liang, C. Lin, J. Lin, H. Qian, D. Qiao, H. Rong, H. Su, L. Sun, L. Wang, S. Wang, D. Wu, Y. Xu, K. Yan, W. Yang, Y. Yang, Y. Ye, J. Yin, C. Ying, J. Yu, C. Zha, C. Zhang, H. Zhang, K. Zhang, Y. Zhang, H. Zhao, Y. Zhao, L. Zhou, Q. Zhu, C.-Y. Lu, C.-Z. Peng, X. Zhu, and J.-W. Pan, "Strong quantum computational advantage using a superconducting quantum processor," 2021.
- [48] C. Zhang, Z. Song, H. Wang, K. Rong, and J. Zhai, "Hyquas: Hybrid partitioner based quantum circuit simulation system on gpu," ser. ICS '21. New York, NY, USA: Association for Computing Machinery, 2021, p. 443–454. [Online]. Available: <https://doi.org/10.1145/3447818.3460357>
- [49] C. Zhang, A. B. Hayes, L. Qiu, Y. Jin, Y. Chen, and E. Z. Zhang, "Time-optimal qubit mapping," in *Proceedings of the 26th ACM International Conference on Architectural Support for Programming Languages and Operating Systems*, 2021, pp. 360–374.
- [50] H.-S. Zhong, H. Wang, Y.-H. Deng, M.-c. Chen, L.-C. Peng, Y.-H. Luo et al., "Quantum computational advantage using photons," 12 2020.